Int. J. Multiphase Flow Vol. 13, No. 3, pp. 309–325, 1987
Printed in Great Britain.

0301-9322/87 $3.00 + 0.00

MODELLING OF THE SKIN FRICTION AND HEAT TRANSFER IN TURBULENT TWO-COMPONENT BUBBLY FLOWS IN PIPES

J. L. MARIÉ

Chargé de Recherche au CNRS, Ecole Centrale de Lyon, Laboratoire de Mécanique des Fluides, 36, avenue G. de Collongue, 69131 Ecully, France

(*Received* 11 *March* 1986; *in revised form* 5 *November* 1986)

Abstract—The skin friction and heat transfer in turbulent two-component bubbly flows in pipes are modelled under the following conditions. The flow is assumed to be vertical, steady, fully developed and to circulate in the upward direction. The modelling is based on two main arguments: first the persistence of the logarithmic velocity and temperature profiles near the wall for low values of the void fraction; second the similarity of the modifications caused by the bubbles on these profiles and those created by a grid in a single-phase turbulent boundary layer. The form of the friction and heat-transfer laws derived is in principle valid at low gas concentrations. However, comparisons with the local measurements presently available in this field and with the correlations of Lockhart & Martinelli and Martinelli & Nelson, show that the model works pretty well up to 0.2–0.3 void fractions.

1. INTRODUCTION

As a rule the problems of two-phase two-component friction and heat transfer are highly complex, which results from the diversity of the mechanisms involved. As underlined by Collier (1972), the flow pattern plays an important role, so that each flow regime is often considered and analysed separately in the literature. Unfortunately, as pointed out by Michiyoshi (1978a) in a very complete critical review of the heat-transfer studies, the local characteristics of these various regimes are not always taken into account in such analysis and thus the influence of certain flow parameters is not perfectly understood. Fully aware of this situation, several workers adopt an original point of view and try to calculate the momentum and heat transfers in bubbly flows by modelling the turbulent structure of the liquid. This is the case of Sato *et al.* (1981) and Van der Welle (1981). Both authors write the equations governing the shear stress and heat flux distributions by using an eddy diffusivity subdivided into two terms. One is for the inherent wall turbulence, the other for the velocity fluctuations created by the bubbles. Sato chooses for the latter diffusivity a semi-empirical algebraïc form and approximates the equations by a finite-difference formulation. The velocity and temperature fields are constructed by means of a numerical iterative method. The quantities to be assigned in the program are: the pipe diameter, the liquid mass flow rate and bulk temperature, the α-profile and estimated values for the wall shear stress and heat flux. The velocity and temperature distributions are computed at each iteration. Finally, the liquid mass flow rate and bulk temperature are deduced and compared with prescribed values. The process is repeated, until consistent velocity and temperature fields are obtained. Van der Welle solves the shear stress equation in a reverse way. The velocity gradient at the surface is first determined by a simple method, well-tested in single-phase flows, but whose extension to gas–liquid flows is somewhat questionable. The value obtained is then substituted in this equation. The eddy diffusivity associated with bubble-induced pseudo-turbulence is derived by identifying the resulting expression with available experimental data on two-phase frictional pressure loss.

The present paper deals with steady fully-developed upward bubbly flows in vertical pipes or channels. It proposes a rather different approach based on a local turbulence description. The latter is supported by the detailed measurements of Lance & Bataille (1982). In turbulent flow, any alteration of the skin friction drag or heat diffusion can be detected by a change in the velocity and temperature profiles within the boundary layers. In this perspective, it is therefore worth knowing whether the bubbles can originate such a change by influencing turbulence and whether the latter change is significant. There are presently a few experimental studies which enable us to

answer this question. Measurements by Serizawa *et al.* (1975) clearly indicate that in a low-quality upward bubbly flow in a pipe, the normal 1/7 power velocity profile is modified. The velocity near the pipe axis is hardly affected, but as one moves towards the surface, the shape becomes flatter, which results in more important gradients at the wall. This difference with turbulent single-phase flows is confirmed by various authors, such as Ohba *et al.* (1976) and Sato *et al.* (1981). The data of the latter authors are particulary interesting because they are the only ones to be plotted in the standard non-dimensional form $U/U^* = f(Y_-)$. In this form, it is noted that the logarithmic distribution persists with its usual slope and constant, whereas the initial wake function is strongly depressed. Now the same behaviour is observed in a single-phase turbulent boundary layer submitted to the action of a grid (Hancock 1980). It is tempting to conclude that the mechanism by which the profile is modified is connected with an increase in the external turbulence, as for the grid. We use this analogy and our knowledge of bubble-induced pseudo-turbulence to develop a simple model which predicts the resulting increases in the friction and heat-transfer coefficients. The efficiency of this model is validated by comparison with a few experiments and correlations.

2. BASES OF THE MODELLING

The bases of the modelling are now examined in detail. Figure 1 shows the velocity modifications caused by the bubbles, according to measurements by Sato *et al.* (1981). Very close to the wall, the void fraction is rigorously null which means that this part of the flow is entirely free of bubbles. As a consequence, the viscous sublayer still exists and here the velocity is given by the well-known linear velocity distribution

$$\frac{\overline{U_L}^x}{U_L^*} = \frac{YU_L^*}{\nu_L} = Y_-, \qquad [1]$$

where subscript L = liquid, Y = distance from the wall, ν = kinematic viscosity, superscript * = friction scales

$$\left(U_L^* = \sqrt{\nu_L \left(\frac{\mathrm{d}\overline{U_L}^x}{\mathrm{d}y}\right)_{y=0}} = \text{new friction velocity}\right)$$

and the operator —x denotes the usual phasic average (Ishii 1975).

Above the sublayer, the void fraction increases up to a maximum by a mechanism which is still not completely understood. Due to the presence of the gas, the standard logarithmic profile is translated downward, indicating that the turbulence moves nearer to the wall. However, at low

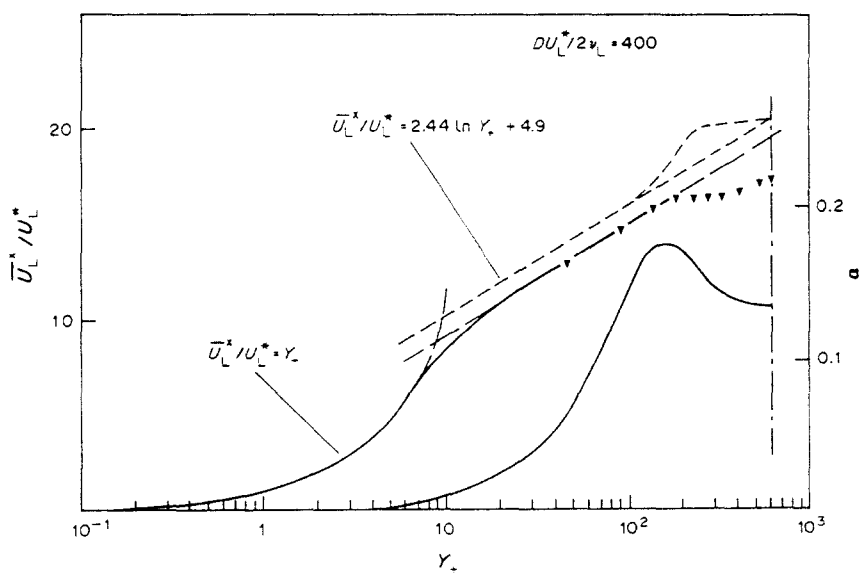

Figure 1. Mean velocity and void fraction profiles (Sato *et al.* 1981) in an upward bubbly flow in a pipe; ——, single-phase flow.

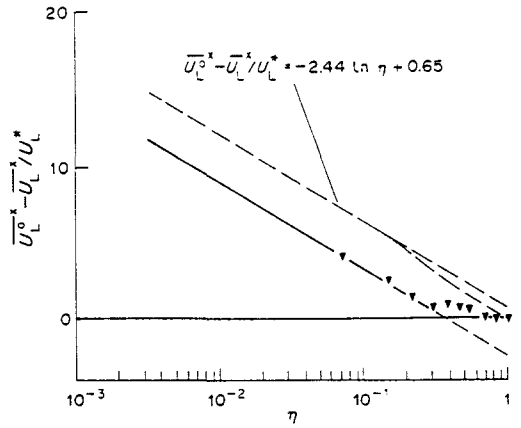

Figure 2. Defect velocity profile drawn from the data of Sato *et al.* (1981); ——, single-phase flow.

air qualities (figure 1) the translation is so slight that it is negligible. Therefore, we can consider that the velocity is still governed by

$$\frac{\overline{U_L}^x}{U_L^*} = \frac{1}{K} \ln Y_+ + C, \qquad [2]$$

where K and C stand for the usual constants. To the contrary, a significant change is exhibited in the core region. The wake function is strongly depressed, as also happens in a turbulent boundary layer submitted to an external turbulence (Hancock 1980). The result is that the wake strength Π_L [defined by Coles (1956)] in the logarithmic defect law is depressed too and becomes negative (figure 2). The corresponding shift of the velocity profile can be written as

$$\frac{\overline{U_L^0}^x - \overline{U_L}^x}{U_L^*} = -\frac{1}{K} \ln \eta + \frac{2\Pi_L}{K}, \qquad [3]$$

where Π_L is inferior to the value Π without bubbles. Superscript 0 refers to the pipe axis and η is the ratio of Y to the pipe radius R. By analogy with the velocity, we expect in this region a similar effect on the profiles of temperature and, hence, equations in the form

$$\frac{\overline{\theta_W} - \overline{\theta_L}^x}{\theta_L^*} = \frac{1}{K_\theta} \ln Y_+ + C_\theta \qquad [4]$$

and

$$\frac{\overline{\theta_L}^x - \overline{\theta_L^0}^x}{\theta_L^*} = -\frac{1}{K_\theta} \ln \eta + \frac{2\Pi_{\theta L}}{K_\theta}, \qquad [5]$$

where subscript W = wall, subscript θ = temperature, K_θ, C_θ = constants in single-phase flows $\Pi_{\theta L}$ = new value of the wake strength Π_θ ($\Pi_{\theta L} < \Pi_\theta$) and θ_L^* is the new friction temperature defined by

$$\theta_L^* = \frac{\phi_W}{\rho_L c_{pL} U_L^*} \qquad [6]$$

in which ϕ = heat flux, ρ = density and c_p = specific heat. Under these conditions, the laws of friction and heat transfer, respectively, read

$$\frac{\overline{U_L^0}^x}{U_L^*} = \sqrt{\frac{2}{CF_L}} = \frac{1}{K} \ln Re_L \sqrt{\frac{CF_L}{2}} + C + \frac{2\Pi_L}{K} \qquad [7]$$

and

$$\frac{St_L}{\frac{CF_L}{2}} = \frac{Nu_L}{Re_L Pr_L \frac{CF_L}{2}} = \frac{\frac{K_\theta}{K}}{1 + \sqrt{\frac{CF_L}{2}} \left(\frac{C_\theta K_\theta - CK + 2\Pi_{\theta L} - 2\Pi_L}{K} \right)}, \qquad [8]$$

where CF = friction coefficient, Re = Reynolds number based on the velocity at the centre of the pipe, Pr = laminar Prandtl number, Nu and St = the Nüsselt and Stanton number, respectively. The term on the r.h.s. of [8] is a general expression for the Reynolds analogy factor (Simonich & Bradshaw 1978). It depends on Pr_L through C_ϑ. At this level, it is clear that the determination of the two laws is equivalent to knowing the strength Π_L and $\Pi_{\vartheta L}$ related to the wake change caused by the bubbles. So as a first step, we need to find the parameters which they depend on. For that purpose, an extension of the dimensional analysis valid for turbulent wall-bounded shear flows (Tennekes & Lumley 1972) is used. This extension is presented in detail in the Appendix. It leads to the following conclusions. First, in the core of the flow, there is a subregion located away from the pipe axis and close to the outer edge of the wall layer, where the action of the bubbles on the wall turbulence is described by two adimensional groups L_B^s/R and $\tilde{u}_B^s/U_L^*$; superscript s stands for the subregion and subscript B for the bubbles, L_B^s is the integral length scale of the eddies generated by the wall. By their kinetic energy, the bubbles tend to break these large eddies and hence to reduce their size. Therefore, L_B^s is probably smaller than in single-phase flows; $\tilde{u}_B^s$ denotes the velocity scale of the fluctuations created by the bubbles. Second, the defect velocity profile in the subregion is expected to be given by a similarity law of the form

$$\frac{\overline{U_L^0}^x - \overline{U_L}^x}{U_L^*} = F\left(\eta, \frac{L_B^s}{R}, \frac{\tilde{u}_B^s}{U_L^*}\right). \qquad [9]$$

As a result, a matching of this profile with that, unaffected, of the inner layer necessarily implies

$$\Pi_L = \Pi_L\left(\frac{L_B^s}{R}, \frac{\tilde{u}_B^s}{U_L^*}\right) \qquad [10]$$

and, by analogy,

$$\Pi_{\theta L} = \Pi_{\theta L}\left(\frac{L_B^s}{R}, \frac{\tilde{u}_B^s}{U_L^*}\right). \qquad [11]$$

The previous relations suggest that the basic mechanism responsible for the wake change is the increase in the velocity fluctuations created by the bubbles. This is not surprising from a physical point of view. As a matter of fact, the momentum transfer being enhanced, it means that the mean velocity profile becomes flatter and subsequently, its wake component progressively vanishes. Such a behaviour is very similar to that observed when a grid turbulence is generated outside a single-phase boundary layer. This analogy incites us to identify the action of the bubbles with that of a fictitious grid, with a random mesh, which would increase the turbulence in the outer layer. Unfortunately, the data presently available in the field of bubbly flows are too incomplete for the functional dependence of Π_L and $\Pi_{\theta L}$ on their arguments to be specified. The original idea of this paper consists of using the above-mentioned analogy, and hence the results relative to single-phase flows, to estimate these unknown functions. The first data concerning the effect of a free-stream turbulence on a boundary layer were reported about 20 years ago in the pioneer work of Kestin *et al.* (1961), and later in the studies of Charnay *et al.* (1971) and Bradshaw (1974). Since then, more detailed information has been published by Simonich & Bradshaw (1978), Hancock (1980), Blair (1983) and Castro (1984). Hancock's experiments, which are well-documented, were performed in a turbulent boundary layer on a flat plate, beneath a nearly homogeneous isotropic grid-generated turbulence. His results clearly indicate that the existence of external velocity fluctuations initiates and increase in the skin friction, in proportion to the scale $\tilde{u}_e$ of these fluctuations, but also on the integral length scale L_e "impressed" on the outer layer by the turbulence. This influence of L_e was not examined in the previous works. The same behaviour is quoted for the heat-transfer coefficient (Simonich & Bradshaw 1978; Blair 1983). In both cases, the increase is related to a depression of the wake strength on the corresponding logarithmic defect profiles. Neglecting the Reynolds number effects, this may be represented by the adimensional laws of the type

$$\Pi_e = \Pi_e\left(\frac{L_e}{\delta_e}, \frac{\tilde{u}_e}{U_e^*}\right) \qquad [12]$$

and

$$\Pi_{\theta e} = \Pi_{\theta e}\left(\frac{L_e}{\delta_e}, \frac{\tilde{u}_e}{U_e^*}\right), \qquad [13]$$

where subscript e denotes the external grid turbulence and δ the boundary layer thickness. The parameter range covered by Hancock's study is $\tilde{u}_e/\overline{U_e} \leqslant 0.07$, where $\overline{U_e}$ = external mean velocity, $0.7 \leqslant L_e/\delta_e \leqslant 4.9$ and $Re_{\delta'} > 2000$, where $Re_{\delta'}$ = Reynolds number based on momentum thickness δ'. In this range, the skin friction increases in a roughly linear way and then rapidly begins to saturate. As noted by Castro (1984), the data suggest that the saturation process is probably due to the persistence of the "log-law" which restricts further change in the mean flow properties, above a certain turbulent intensity. Accordingly, [12] and [13] can be expected to be valid in bubbly flows provided that L_e/δ_e is replaced by L_B^s/R and $\tilde{u}_e/U_e^*$ by $\tilde{u}_B^s/U_L^*$. Then the modelling becomes simple. Knowing Π_e and $\Pi_{\theta e}$, the two terms to be expressed are L_B^s/R and $\tilde{u}_B^s/U_L^*$. They can be determined by means of the experimental results of Lance *et al.* (1984) and Michiyoshi & Serizawa (1985). In a second step, it is necessary to check that the form of Π_L and $\Pi_{\theta L}$ obtained by substitution of the variables is consistent with measurements by Sato *et al.* (1981). The final step is the derivation of the laws of friction and heat transfer and their comparison with experimental data.

The laws of variation of the wake strength Π_e and $\Pi_{\theta e}$ are not reported in the literature. Consequently, they must be inferred from the experimental curves describing the increases in CF_e/CF and St_e/St. To do that, we need *a priori* two relations, one between Π_e and CF_e/CF and another one between $\Pi_{\theta e}$ and St_e/St. But, as proved by Blair's (1983) study, the wake depressions observed on the velocity and temperature profiles are quantitatively similar, whatever the intensity of the free-stream turbulence generated ($\tilde{u}_e/\overline{U_e} \leqslant 0.06$). Thus,

$$\Delta\Pi_{\theta e} = \frac{2}{K}(\Pi_{\theta e} - \Pi_\theta) \sim \Delta\Pi_e; \qquad [14]$$

the second relation is in fact useless. From the friction laws, with and without external turbulence (Bradshaw 1974), one can show that for boundary layers with the same $U^*\delta/\nu$,

$$\sqrt{\frac{CF_e}{CF}} \sim 1 - \frac{2}{K}(\Pi_e - \Pi)\sqrt{\frac{CF_e}{2}}. \qquad [15]$$

The second term on the r.h.s. is typically of the order of 0.2, so that

$$\left(\frac{CF_e}{CF}\right)_{\frac{U^*\delta}{\nu}\,\text{const}} \sim 1 - \frac{4}{K}(\Pi_e - \Pi)\sqrt{\frac{CF_e}{2}}. \qquad [16]$$

In most experiments, CF_e/CF is measured at $\overline{U_e}\delta'/\nu$ const. As indicated in figure 3, a significant scatter exists in the experimental data. For the sake of simplicity, it is chosen to approximate the trend exhibited by Hancock's data by a straight line, the equation of which is

$$\left(\frac{CF_e}{CF}\right)_{\frac{\overline{U_e}\delta'}{\nu}\,\text{const}} \sim 1 + \frac{14}{\frac{L_e}{\delta_e} + 2}\frac{\tilde{u}_e}{\overline{U_e}}. \qquad [17]$$

Such an approximation is relevant because it includes the aforementioned saturation process. The latter occurs when FSTP > 1. FSTP stands for the free-stream turbulence parameter introduced by Hancock to correlate his data. The question is how to connect [16] with [17]. Robertson & Holt's (1972) measurements suggest that the correlation between the change in the boundary layer thickness and the change ΔCF in the skin fraction coefficient can be roughly fitted by

$$\frac{\frac{\delta}{\delta'}}{\frac{\delta_0}{\delta_0'}} \sim 1 + 1.5\left(\frac{\Delta CF}{CF}\right)_{\frac{\overline{U_e}\delta'}{\nu}\,\text{const}} \qquad [18]$$

for $\tilde{u}_e/\overline{U_e} \leqslant 0.06$. Bradshaw used this correlation to convert the increase of skin friction at const $\overline{U_e}\delta/\nu$, given by Charnay *et al.* (1971), to an increase at const $\overline{U_e}\delta'/\nu$. Following his method, we find that the coefficient of proportionality in $(CF_e/CF)_{\frac{\overline{U_e}\delta}{\nu}\,\text{const}}$ is smaller by 15/4 than for the ratio

at constant $\overline{U_e}\delta'/\nu$, that is

$$\left(\frac{CF_e}{CF}\right)_{\frac{\overline{U_e}\delta}{\nu}\text{ const}} \sim 1 + \frac{10}{\frac{L_e}{\delta_e} + 2}\frac{\tilde{u}_e}{U_e}. \qquad [19]$$

The accuracy of such a conversion is of the same order as for correlation [18], i.e. about 10%. In addition, Bradshaw demonstrated that the difference between the skin friction ratio at $\overline{U_e}\delta/\nu$ const and its value at $U^*\delta/\nu$ const remains of the order 0.1, i.e. of the same order as the measurement errors. So, we can identify [16] and [19] and write, within 10–20% error,

$$\Delta\Pi_e = \frac{2}{K}(\Pi_e - \Pi) \sim -\frac{5}{\frac{L_e}{\delta_e} + 2}\frac{\tilde{u}_e}{U_e^*}. \qquad [20]$$

Since $\Delta\Pi_e$ and hence $\Delta\Pi_{\theta e}$ are known, the corresponding increase in Stanton number can be also calculated. According to [8], the Reynolds analogy factor is expressed by

$$\frac{\frac{St_e}{CF_e}}{\frac{2}{2}} = \frac{\frac{K_\theta}{K}}{1 + \sqrt{\frac{CF_e}{2}}\left(\frac{C_\theta K_\theta - CK + 2\Pi_{\theta e} - 2\Pi_e}{K}\right)}. \qquad [21]$$

Defining the quantity p_r by

$$p_r = \frac{C_\theta K_\theta - CK + 2\Pi_\theta - 2\Pi}{K} \qquad [22]$$

and substituting [15] in [21] yields, to the first order in $\Delta\Pi_e$, $\Delta\Pi_{\theta e}$,

$$\frac{\frac{St_e}{CF_e}}{\frac{2}{2}} \sim \frac{\frac{K\theta}{K}}{1 + p_r\sqrt{\frac{CF}{2}} + \left[\Delta\Pi_{\theta e} - \Delta\Pi_e\left(1 + p_r\sqrt{\frac{CF}{2}}\right)\right]\sqrt{\frac{CF_e}{2}}}; \qquad [23]$$

from which we deduce

$$\frac{St_e}{St} \sim \frac{1 - 2\Delta\Pi_e\sqrt{\frac{CF_e}{2}}}{1 + \left(\frac{\Delta\Pi_{\theta e}}{1 + p_r\sqrt{\frac{CF}{2}}} - \Delta\Pi_e\right)\sqrt{\frac{CF_e}{2}}}. \qquad [24]$$

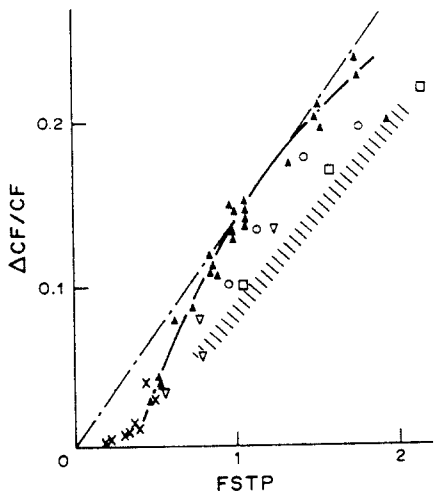

Figure 3. Experimental evolution of ΔCF/CF. FSTP = $100\,\tilde{u}_e/\overline{U_e}\,(L_e/\delta_e + 2)$. Solid symbols, Hancock's (1980) measurements; open symbols and ×, other author's data; (▨), data of Charnay *et al.* (1971); ——, Hancock's correlation curve.

Arguing that the second term in the denominator is negligible with respect to unit and retaining only the first order in $\sqrt{CF_e/2}$, we get

$$\left(\frac{St_e}{St}\right)_{\frac{U_e\theta}{\nu}\,\text{const}} \sim \left(\frac{St_e}{St}\right)_{\frac{U_e\delta}{\nu}\,\text{const}} \sim 1 - \left(\Delta\Pi_e + \frac{\Delta\Pi_{\theta e}}{1 + p_r\sqrt{\frac{CF}{2}}}\right)\sqrt{\frac{CF_e}{2}}. \qquad [25]$$

The equality between the wake strength variations ([14]) implies

$$\left(\frac{St_e}{St}\right)_{\frac{U_e\theta}{\nu}\,\text{const}} \sim 1 - 2\Delta\Pi_e \left(\frac{1 + \frac{p_r}{2}\sqrt{\frac{CF}{2}}}{1 + p_r\sqrt{\frac{CF}{2}}}\right)\sqrt{\frac{CF_e}{2}}, \qquad [26]$$

which is equivalent to

$$\left(\frac{St_e}{St}\right)_{\frac{U_e\theta}{\nu}\,\text{const}} \sim \frac{10}{\frac{L_e}{\delta_e} + 2}\left(\frac{1 + \frac{p_r}{2}\sqrt{\frac{CF}{2}}}{1 + p_r\sqrt{\frac{CF}{2}}}\right)\frac{\tilde{u}_e}{\overline{U_e}}. \qquad [27]$$

We have now all the necessary elements for the laws of friction and heat transfer to be derived.

3. DERIVATION OF THE LAWS OF SKIN FRICTION AND HEAT TRANSFER

The main difficulty is the modelling of L_B^s/R and $\tilde{u}_B^s/U_L^*$. Recent data obtained by Michiyoshi & Serizawa (1984) confirm that L_B^s/R decreases as the void fraction α increases. This is evidence that the large eddies are broken into smaller structures by the bubble agitation effect. Unfortunately, due to the important scatter of the data, it is difficult to find a law which characterizes the α-dependence of the integral length scale. As a first approximation, the decrease can be roughly considered as linear and represented by

$$\frac{L_B^s}{R} \sim 1 - 3\alpha^s. \qquad [28]$$

In fact, the dependence is probably more complex and should perhaps include other parameters, such as the ratio between the bubble diameter and the pipe radius. Without any additional measurements, more assertive conclusions cannot be drawn. Thus [28] is adopted.

Regarding the turbulence, the experiments of Lance & Bataille (1982) exhibit an important fact. They prove that the amplitude of the fluctuations created by the bubbles is strongly determined by the intensity $\sqrt{\overline{u^2}}$ of the fluctuations existing in the liquid before the air injection. At low turbulent intensity, Lance *et al.* (1984) show that it is possible to calculate this amplitude from the velocity field around an isolated bubble. They find that in the longitudinal direction

$$\sqrt{\overline{u_B^2}} = \sqrt{k\alpha}\,\overline{U_R}^x, \qquad [29]$$

where $k(0.8 \leqslant k \leqslant 1.4)$ depends on the value of the parameters governing the trajectory of the bubble and $\overline{U_R}^x$ denotes its relative velocity. For certain applications, it is convenient to adopt an average value of k. We see in figure 4 that the choice $k = 1.1$ fits quite satisfactorily the fluctuations measured by hot-film anemometry (Lance & Bataille 1982) or LDA (Marié 1983). In theory, [29] is only valid for very low void fractions. As a matter of fact, it does not account for the hydrodynamic interactions between the bubbles, which would involve an additional term of order α^2. Nevertheless, the experiments of Aoki (1982) and Michiyoshi & Serizawa (1984) show that the contribution of this term to the total bubble-induced pseudo-turbulence remains rather small up to gas concentrations of 10%. Assuming, in order to simplify, that the fluctuations generated by

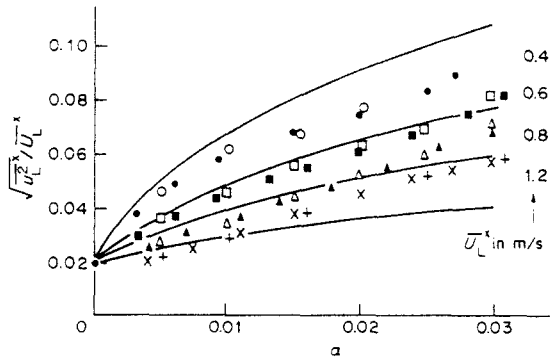

Figure 4. Turbulent intensity in the presence of bubbles:

$$\frac{\sqrt{\widetilde{u_L^2}^x}}{\overline{U_L}^x} = \frac{\sqrt{\widetilde{u_B^2} + \overline{u^2}}}{\overline{U_L}^x}$$

Solid symbols, measurements by hot-film anemometry; open symbols, LDA measurements; ——, [29] with $k = 1.1$, $\overline{U_L}^x = 0.25$ cm/s.

the bubbles are quasi-isotropic, it is then possible to take $\tilde{u}_B^s$ equal to $\sqrt{\widetilde{u_B^2}}$ and express u_B^s/U_L^* as

$$\frac{\tilde{u}_B^s}{U_L^*} = \sqrt{k\alpha^s}\,\frac{\overline{U_R^s}^x}{U_L^*}. \qquad [30]$$

Substituting [28] and [30] in [20], we finally obtain

$$\Delta\Pi_L = \frac{2}{K}(\Pi_L - \Pi) \sim -\frac{5}{3(1-\alpha^s)}\sqrt{1.1\alpha^s}\,\frac{\overline{U_R^s}^x}{U_L^*}. \qquad [31]$$

Let us see if this equation is consistent with the measurements of Sato *et al.* (1981). The values of the flow parameters corresponding to figure 3 are J_L (superficial velocity) = 0.5 m/s, $\alpha^s = 0.15$ and $U_L^* = 0.038$ m/s. There is no indication of the value of the slip velocity. However, $\overline{U_R^s}^x = 0.18$ m/s seems to be a reasonable estimate, considering the experimental conditions. The shift in the wake strength calculated from these data is $\Delta\Pi_L = -3.8$, while the value determined from the velocity profile is -3.2.

The agreement is quite good which tends to prove that the assimilation of the effect of the bubbles with that of a grid is physically relevant. This is an argument to write the resulting laws of friction and heat transfer. Replacing $\Delta\Pi_e$ by $\Delta\Pi_L$ in [16] and [26] gives

$$\frac{CF_L}{CF} \sim 1 + \frac{10}{3(1-\alpha^s)}\sqrt{1.1\alpha^s}\,\frac{\overline{U_R^s}^x}{\overline{U_L^0}^x} \qquad [32]$$

and

$$\frac{St_L}{St} \sim 1 + \frac{10}{3(1-\alpha^s)}\left(\frac{1 + \frac{p_r}{2}\sqrt{\frac{CF}{2}}}{1 + p_r\sqrt{\frac{CF}{2}}}\right)\sqrt{1.1\alpha^s}\,\frac{\overline{U_R^s}^x}{\overline{U_L^0}^x}. \qquad [33]$$

At this level, it must be stressed that [17] and [29] are expressions whose validity is experimentally established over the respective ranges $\tilde{u}_e/\overline{U_e} = 0 - 0.07$ and $\alpha < 0.10$. For this reason, and due to the approximations introduced in the derivation of [20] and [27], [32] and [33] are expected to work *a priori* better at low values of the void fraction. To discuss this point and illustrate the efficiency of the model a comparison with experiments is now presented.

4. COMPARISON WITH EXPERIMENTS

Since the model takes into account the local properties of the flow, it is appropriate for the comparison to choose the experiments in which the local increase in skin friction and heat transfer is measured. Such experiments are not numerous in the literature.

4.1. Skin friction

Quite recently Souhar (1979), carried out an experimental study of the local wall shear stress in bubbly and slug regimes. The flow is circulating upward through a 44 mm i.d. vertical tube at atmospheric pressure and a regulated temperature of 291 K. The gas is axially injected through a conic mixer placed at the bottom of the tube. All the measurements are performed by means of a polarographic method (Lebouché & Cognet 1967) in a section located at $Z/D = 120$ (Z = streamwise coordinate, D = pipe diameter). At this distance, one can agree with Herringe & Davis (1976) that the flow is developed. The increase in wall shear stress is measured at various superficial liquid velocities J_L between 0.15 and 1.35 m/s and various gas qualities X between $0.27 \cdot 10^{-4}$ and 0.0263. The main difficulty when trying to compare these measurements with [32] is to find how to relate the local variables $\overline{U_L^0}^x$, α^s and $\overline{U_R^s}^x$ to the control parameters J_L and X. Concerning the liquid velocity, the data of Serizawa *et al.* (1975) prove that at low gas qualities, $\overline{U_L^0}^x$ is equal to $\overline{U^0}$ or sometimes lower. Consequently, it is reasonable to assume $\overline{U_L^0}^x \sim J_L$. For the void fraction, the problem is more complex. Indeed saddle-shape or power law void fraction distributions are observed according to the investigators and their inlet geometry.

In the saddle-shape pattern (figure 1) the void fraction profile exhibits a peak near the wall at a Y/R location of about 0.1–0.3. This coincides precisely with the location of the subregion previously referenced by the superscript s, so that

$$\alpha^s = \alpha_1^s = \alpha_{peak}. \tag{34}$$

In the second pattern, Van der Welle (1985), in agreement with other authors, shows that the gas distributions are well-fitted by

$$\alpha = \alpha_{max}\left(1 - \frac{r}{R}\right)^{\frac{1}{n}} \tag{35}$$

or, equivalently, by

$$\alpha = \langle\alpha\rangle \frac{1}{2}\left(1 + \frac{1}{n}\right)\left(2 + \frac{1}{n}\right)\left(1 - \frac{r}{R}\right)^{\frac{1}{n}}, \tag{36}$$

where the operator $\langle\ \rangle$ denotes the cross-sectional average. As a result,

$$\alpha^s = \alpha_2^s \sim \langle\alpha\rangle \frac{1}{2}\left(1 + \frac{1}{n}\right)\left(2 + \frac{1}{n}\right) 0.2^{\frac{1}{n}}. \tag{37}$$

There is considerable scatter in constant n since it may vary from 0.1 to 7. Choosing an average value $n = 3.5$ yields $\alpha_2^s = 0.93\langle\alpha\rangle$. Thus, $\alpha_1^s > \alpha_2^s$ and it follows that the distinction between the two patterns is essential. Unfortunately, in most experiments presented here, information about the shape of the void fraction profile are missing or incomplete. In particular, when a saddle-shape exists, the value of α_{peak} is not systematically given. Under those conditions we have no other alternative but to take $\alpha^s = \langle\alpha\rangle$, whatever the gas distribution, and to keep in mind that this choice is appropriate to power law α profiles. Having outlined this, it remains to express $\overline{U_R^s}^x$. For 1-D vertical upward bubbly flows, Zuber & Hench (1962) propose to use the relationship

$$\overline{U_R}^x = U_\infty (1 - \alpha)^{\frac{1}{2}}, \tag{38}$$

where U_∞ is the terminal velocity of an isolated bubble rising in an infinite medium and $(1-\alpha)^{1/2}$ is a corrective term to take into account the bubble interactions. From all these arguments, we finally get

$$\frac{CF_L}{CF} \sim \frac{\overline{\tau_{WL}}^x}{\overline{\tau_W}} \sim 1 + \frac{10}{3(1 - \langle\alpha\rangle)}\sqrt{1.1\langle\alpha\rangle(1 - \langle\alpha\rangle)}\,\frac{U_\infty}{J_L}, \tag{39}$$

where τ_W is the wall shear stress.

In Souhar's experiment, the gas injected is nitrogen and the liquid is an electrolyte which has the same physical properties as pure water. No information on bubble size is given. However, according to the nature of the injection system and the range of liquid flow rate, one may estimate their mean diameter to be of the order of 3–5 mm. Under such conditions, the terminal velocity of these bubbles is probably the same as for equivalent air bubbles in water, i.e. $U_\infty = 0.25$ m/s (Clift

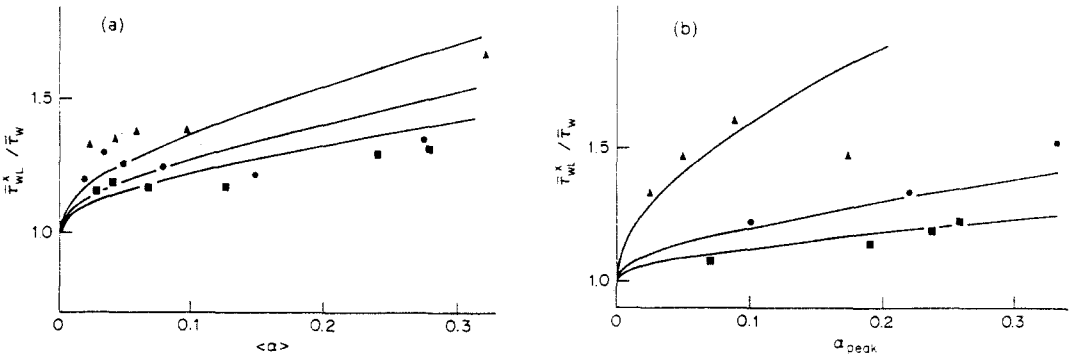

Figure 5a. Evolution of $\overline{\tau_{WL}}^{x}/\overline{\tau_W}$. Symbols – Souhar's (1979) measurements; $J_L = 0.8$ m/s (▲), $J_L = 1.08$ m/s (●) $J_L = 1.35$ m/s (■). Curves – predicted values, $U'_\infty = 0.25$ m/s.

Figure 5b. Evolution of $\overline{\tau_{WL}}^{x}/\overline{\tau_W}$. Symbols – Souhar's (1981) measurements; $J_L = 0.5$ m/s (▲), $J_L = 1.5$ m/s (●) $J_L = 2.5$ m/s (■). Curves – predicted values, $U'_\infty = 0.25$ m/s.

et al. 1978). The calculation of $\overline{\tau_{WL}}^{x}/\overline{\tau_W}$ with this value yields the curves in figure 5a. The symbols represent the results of Souhar after the gas quality X has been converted into $\langle\alpha\rangle$ by the Wallis (1969) relationship

$$X = \frac{\rho_G\langle\alpha\rangle\,[J_L + (1-\langle\alpha\rangle)\overline{U_R}^{x}]}{[\rho_L(1-\langle\alpha\rangle) + \rho_G\langle\alpha\rangle]J_L + \rho_G\langle\alpha\rangle(1-\langle\alpha\rangle)\overline{U_R}^{x}}. \qquad [40]$$

Roughly speaking, the agreement between the measurements and the prediction is not too bad. The curves and the symbols are pretty well concentrated around an average value $\overline{\tau_{WL}}^{x}/\overline{\tau_W} = 1.3$. However, the real tendency is not perfectly reflected by the prediction. Souhar finds that the wall shear stress ratio rises sharply, reaches an asymptotic level and sometimes decreases while, according to our theory the increase in turbulence and hence in wall shear stress, is much more gradual and continuous. In fact, these behaviour differences are not difficult to understand. Souhar's measurements correspond to flows with saddle-shaped void fraction profiles for which [39] is not very well adapted. The proof is given by additional data obtained later (Souhar 1981) using the same facility, equipped with an annular wall injection. Measurements of the local void fraction are then systematically presented. They reveal the existence of the peaks and specify for each of the experimental conditions investigated the value of α_{peak}. Thus calculation of $\overline{\tau_{WL}}^{x}/\overline{\tau_W}$ by taking $\alpha^s = \alpha_{peak}$ is possible. It gives the curves in figure 5b. No deviation occurs, as in the previous case, and the agreement is good even at the highest values of the void fraction. The only significant difference is that noted at $J_L = 0.5$ m/s. Indeed, beyond $\langle\alpha\rangle = 0.15$ measurements exhibit a decrease in skin friction which is not predicted by the model. As a rule, such a decrease is observed for superficial velocities < 1.5 m/s (see figure 5a). Over this range "blocking" effects are important and when the gas flow rate exceeds a critical value, recirculations are generated near the wall by the gradients of concentration. The transition to slug flow begins to take place. The negative wall shear stress fluctuations which result, cause the decrease of the algebraic average $\overline{\tau_{WL}}^{x}$. Such a phenomenon has been disregarded in the present modelling.

It is also possible to compare [39] with some global correlations. Of course, such correlations are known for sometimes exhibiting important deviations from experimental data. Thus, they cannot be considered as accurate enough for a reliable validation of the model. However, comparison is interesting because it illustrates the superiority of the present approach regarding the correlations universally used by engineers. Among these correlations, the most famous one is certainly that proposed by Lockhart & Martinelli (1949). Following their approach, the frictional pressure gradient $(d\overline{P_L}^{x}/dZ)_F$ in two-phase flow is obtained by

$$\left(\frac{d\overline{P_L}^{x}}{dZ}\right)_F = \Phi_L^2\left(\frac{d\overline{P}}{dZ}\right)_{FL}, \qquad [41]$$

where $(d\overline{P}/dZ)_{FL}$ is evaluated for the liquid flowing alone in the same tube and with the same flow rate as in two-phase flow; Φ_L^2 is called the Lockhart–Martinelli factor. The momentum balance for

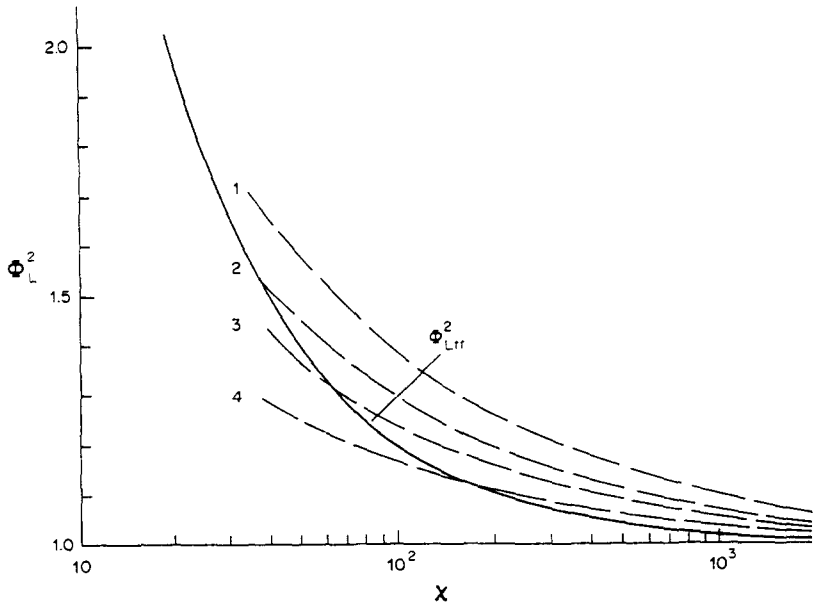

Figure 6. Comparison with the Lockhart–Martinelli correlation: ——, predicted values, $U_x = 0.25$ m/s; (1) $J_L = 0.82$ m/s; (2) $J_L = 1.08$ m/s; (3) $J_L = 1.35$ m/s; (4) $J_L = 2$ m/s.

a pipe flow involves that

$$\left(\frac{d\overline{P_L}^x}{dZ}\right)_F = 4\frac{\overline{\tau_{WL}}^x}{D} \qquad [42]$$

and thus

$$\Phi_L^2 = \frac{\overline{\tau_{WL}}^x}{\overline{\tau_W}}. \qquad [43]$$

The increase in wall shear stress can be calculated from [39] provided that the turbulent Reynolds number $Re_L^* = U_L^* R/\nu_L$ is high enough. For most pipe diameters, this condition is equivalent to assuming that the liquid and the gas are both turbulent. In this case Φ_L^2 is denoted by Φ_{Ltt}^2 and generally approximated by

$$\Phi_{Ltt}^2 \sim 1 + \frac{20}{\chi_{tt}} + \frac{1}{\chi_{tt}^2}, \qquad [44]$$

where

$$\chi_{tt}^2 = \left(\frac{\mu_L}{\mu_G}\right)^{0.25}\left(\frac{1-X}{X}\right)^{1.75}\frac{\rho_G}{\rho_L}. \qquad [45]$$

Subscript G = gas and μ is the viscosity.

The comparison of [39] with [44] is shown in figure 6. The parameter χ_{tt} has been substituted for $\langle\alpha\rangle$ by means of [40]. Quite a correct agreement is observed especially at $J_L = 1.35$ m/s. Above and below this value, the prediction significantly deviates from the curve Φ_{Ltt}^2. This influence of the superficial velocity is still more obvious when considering the correlation of Martinelli & Nelson (1948). The latter is an adaptation of the previous method to steam–water flow. The frictional two-phase pressure drop $(d\overline{P_L}^x/dZ)_F$ is expressed from the frictional pressure drop of the liquid flowing alone in the tube with a flow rate equal to the total flow rate of the two-phase flow:

$$\left(\frac{d\overline{P_L}^x}{dZ}\right)_F = \Phi_0^2\left(\frac{d\overline{P}}{dZ}\right)_{FL0}. \qquad [46]$$

The relationship between Φ_0^2 (Martinelli–Nelson factor) and Φ_{Ltt}^2 reads

$$\Phi_0^2 = (1-X)^{1.75}\Phi_{Ltt}^2. \qquad [47]$$

It is convenient here to introduce the mass velocity

$$G = \rho_G J_G + \rho_L J_L \qquad [48]$$

and to replace $\overline{U_R}^x = U_\infty(1 - \langle\alpha\rangle)^{1/2}$ in [39] by

$$\overline{U_R}^x = \frac{U_D}{(1 - \langle\alpha\rangle)} \sim U_D, \qquad [49]$$

where U_D is a drift velocity. Then we get

$$\frac{\overline{U_R^2}^x}{J_L} \sim \frac{\rho_L U_D}{G(1 - X)} \qquad [50]$$

and $\langle\alpha\rangle$ can be eliminated by using the drift flux model proposed by Zuber & Findlay (1965):

$$\langle\alpha\rangle = \frac{X}{C_0\left[X + (1 - X)\dfrac{\rho_G}{\rho_L}\right] + \dfrac{\rho_G U_D}{G}}, \qquad [51]$$

where C_0 is a constant.

Thus [39] becomes a function of G, ρ_G, ρ_L, U_D and X only and Φ_0^2 can be calculated at various pressures and mass velocities. The possible values for C_0 and U_D are reported in Wallis (1969). Taking $C_0 = 1$ and

$$U_D = 1.53\left|\frac{\sigma g(\rho_L - \rho_G)}{\rho_L^2}\right|^{\frac{1}{4}}, \qquad [52]$$

where σ = surface tension and g = gravity, yields the curves in figure 7 for $P = 68.9$ b. The straight lines represent the variations of Φ_0^2 according to Martinelli & Nelson and the homogeneous model

$$\Phi_0^2 = \left|1 + X\left(\frac{\rho_L}{\rho_G} - 1\right)\right|\left|1 + X\left(\frac{\mu_L}{\mu_G} - 1\right)\right|^{-\frac{1}{4}}. \qquad [53]$$

We note that the theoretical curves coincide with the Martinelli–Nelson correlation when G is small and that they lie close to the homogeneous model as G increases. Now it is known that this model provides more accurate pressure drop estimates in the higher mass velocity ranges ($G > 2000$–2500 kg/m^2 s), while the correlation gives better results in the lower mass velocity range ($G < 1000$ kg/m^2 s). We conclude that the mass velocity is an important parameter whose influence is well taken into account in the present model.

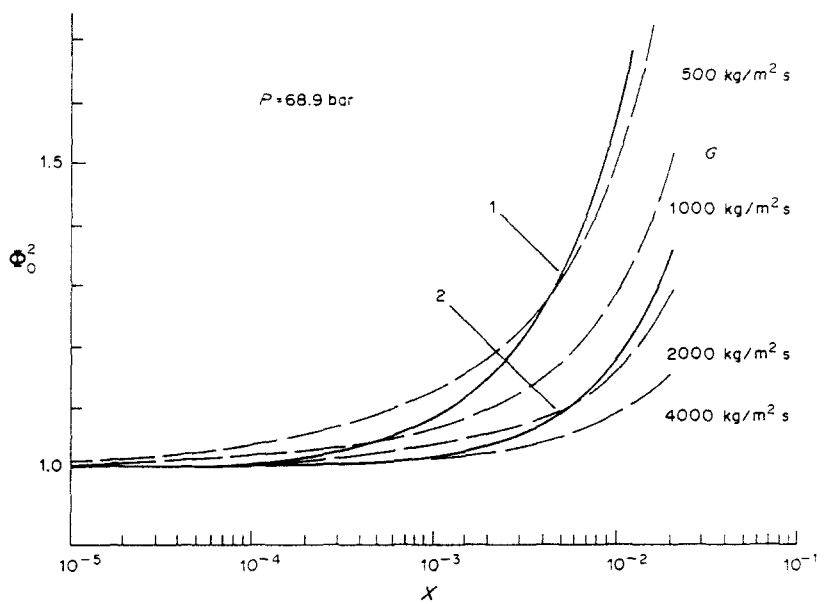

Figure 7. Comparison with the Martinelli–Nelson correlation (1) and the homogeneous model (2); ——, predicted values.

4.2. Heat transfer

Regarding heat transfer, comparison is made with the data obtained by Bobkov *et al.* (1973) in a gas–water pre-mix flowing upward through a 28.9 mm dia vertical pipe. The measuring section is located at $Z/D = 66$ and hence the flow may be considered at almost developed. The temperatures in the gas–water mixture and at the inner surface are determined by means of Chromel–Alumel thermocouples having junctions 0.2 mm dia. The uncertainty of the measurements is estimated to be $<0.1°C$. The nature of the gas, the size of the bubbles and the Prandtl number are not specified. So we suppose that the terminal velocity of the bubbles is of order 0.25 m/s and that Pr is close to 7. Having underlined this, the calculation of the heat transfer increase is performed with the same approximations as in section 4.1, that is

$$\frac{\mathrm{St_L}}{\mathrm{St}} = \frac{h_\mathrm{L}}{h} \sim 1 + \frac{10}{3(1-\langle\alpha\rangle)} \left(\frac{1 + \frac{p_\mathrm{r}}{2}\sqrt{\frac{\mathrm{CF}}{2}}}{1 + p_\mathrm{r}\sqrt{\frac{\mathrm{CF}}{2}}} \right) \sqrt{1.1\langle\alpha\rangle(1-\langle\alpha\rangle)}\,\frac{U_\infty}{J_\mathrm{L}}, \qquad [54]$$

where h = heat-transfer coefficient and CF is determined by the classical formula

$$\frac{\mathrm{CF}}{2} = 0.0395 \left(\frac{J_\mathrm{L} D}{\nu_\mathrm{L}} \right)^{-\frac{1}{4}}, \qquad [55]$$

while p_r is evaluated by taking $K = 0.41$, $K_\theta = 0.47$, $2\Pi/K = 2\Pi_\theta/K_\theta = 0.65$, $C = 4.9$ and C_ϑ under the form suggested by Kader & Yaglom (1972):

$$C_\vartheta = 12.5\,\mathrm{Pr}^{\frac{2}{3}} + 2.12 \ln \mathrm{Pr} - 5.3. \qquad [56]$$

The corresponding curves are shown in figure 8. The symbols denote the experimental data. These data were initially plotted vs the volumetric quality β. The latter has been changed into $\langle\alpha\rangle$ by using the Wallis correlation. The agreement between experiment and prediction is satisfactory which makes any comment pointless. It clearly demonstrates that the model works well up to void fractions of order 0.3, which was unexpected *a priori* owing to the limitations of our model.

From the curves in figures 5a, b and 8, we deduce that $\mathrm{St_L}/\mathrm{St}$ as $\overline{\tau_{\mathrm{WL}}^{\mathrm{x}}}/\overline{\tau_\mathrm{W}}$ increases significantly even when $\langle\alpha\rangle$ is small, exactly as was observed by Lance & Bataille (1982) on the turbulent intensity. On the other hand, the fact that for $\langle\alpha\rangle$ const the increase is greater for the low values of J_L is connected with a similar effect on the turbulence whose explanation can be found in the same reference.

Measurements of local heat transfer have been performed more recently by Michiyoshi (1978b) in an upward air–water flow through a vertical annulus in bubbly and slug regimes. The test section is composed of two concentric cylinders whose diameters are 12 and 52 mm. The inner wall of the annulus is the only one to be heated. Two cases are dealt with: (a) air is mixed with the water stream at the inlet of the annulus; and (b) air is injected into the water stream through small holes at the heater surface. In both configurations the measuring point is located at a distance $Z = 1.8$ m downstream from the inlet of the test section. The bubble diameter is 3 mm and the Prandtl number is equal to 6.56 in case (a) and 7.19 in case (b). Because of the geometry, the calculation of $\mathrm{St_L}/\mathrm{St}$ from [54] seems to be difficult here. Nevertheless, the difficulty is overcome when one considers the

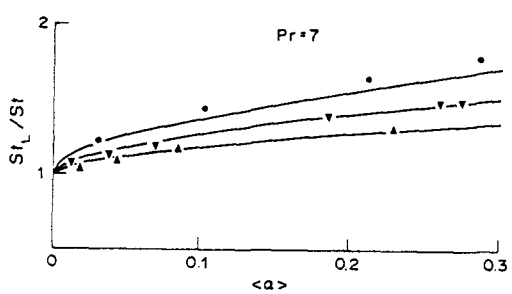

Figure 8. Evolution of $\mathrm{St_L}/\mathrm{St}$. Symbols—measurements of Bobkov *et al.* (1973); $J_\mathrm{L} = 0.52$ m/s (●), $J_\mathrm{L} = 0.71$ m/s (▼), $J_\mathrm{L} = 1.04$ m/s (▲). Curves—predicted values, $U_\infty = 0.25$ m/s.

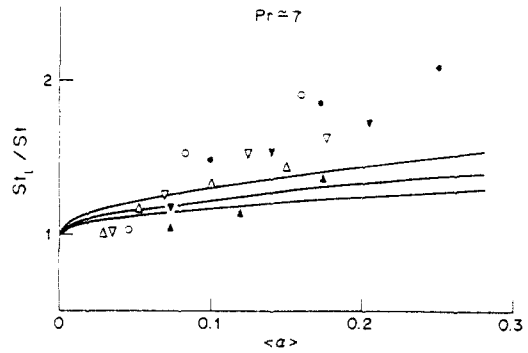

Figure 9. Evolution of St_L/St. Symbols [case (a) = solid symbols, case (b) = open symbols]—Michiyoshi's (1978b) measurements; $J_L = 0.64$ m/s (●○), $J_L = 0.88$ m/s (▼▽), $J_L = 1.14$ m/s (▲△). Curves—predicted values, $U_\infty = 0.25$ m/s.

flow along the inner cylinder as a turbulent boundary layer on a flat plate. Then, referring to Schlichting (1960), CF is given by

$$\frac{CF}{2} = 0.0296\left(\frac{U_{Le}^{x}Z}{\nu_L}\right)^{-\frac{1}{5}}, \qquad [57]$$

whereas p_r is determined by taking $2\Pi/K = 2\Pi_\theta/K_\theta = 2.35$. The result is the curves in figure 9. The symbols represent the data of Michiyoshi (1978b). As in Bobkov *et al.* (1973), $\langle\alpha\rangle$ has been substituted for the volumetric quality β.

We note that the theory provides values which are generally lower than the experimental data. This is explained by three different reasons. The first is obviously the simplication introduced in the calculation by approximating the cylinder by a flat plate, but this is not the most sensitive. The second is the error made by neglecting the void fraction peaks. Here we know from measurements that such peaks exist and that there amplitude is larger in case (b) than in case (a). This is precisely why the heat-transfer coefficients in figure 9 are larger in case (b). The last reason is that the flow is certainly more complex than expected which, according to Fernholtz & Vagt's (1981) observations, could be due to the existence of extra phenomena, such as swirling effects, tridimensionality of the boundary layers, separation, a.s.o. Under such conditions, it is not suitable to emphasize the discrepancy between prediction and experiment.

5. CONCLUSION

Through an original approach, we derive the laws of friction and heat transfer for turbulent two-component upward bubbly flows in vertical pipes. This approach is essentially based on turbulence considerations. A simple model developed within this framework provides the increase of drag and heat-transfer coefficients for arbitrary values of the Prandtl number, the mean void fraction $\langle\alpha\rangle$ and the mean velocities of the two phases. Comparison with experimental data exhibits fairly good agreement up to void fractions of order 0.3. Such a model could still be improved if the action of the bubbles on the integral length scale of wall turbulence were better evaluated. For that purpose, it would be essential to dispose of detailed measurements in which the influence of the void fraction, the bubble diameter and the pipe radius would be systematically isolated and analysed.

Acknowledgement—The author expresses his gratitude to Dr Lance for his useful comments.

REFERENCES

AOKI, S. 1982 Eddy diffusivity of momentum in bubbly flow. M.S. Thesis, Kyoto Univ., Kyoto, Japan (in Japanese).

BLAIR, M. F. 1983 Influence of free-stream turbulence on turbulent boundary layer heat transfer and mean profile development. Parts I & II. *ASME Jl Heat Transfer* **105,** 33–47.

BOBKOV, V. P., IBRAGIMOV, M. K., TYCHINSKII N. A. & FEDOTOVSKII, V. S. 1973 Thermal diffusion in a turbulent water stream with gas bubbles. *Zhenerno Fiz. Zh.* **24,** 551–557.

BRADSHAW, P. 1974 Effect of free-stream turbulence on turbulent shear layers. Aeronautical Research Council Paper 35648, pp. 1–12.

CASTRO, I. P. 1984 Effects of free-stream turbulence on low Reynolds number boundary layers. *ASME Jl Fluid Engng* **106,** 298–306.

CHARNAY, G., COMTE-BELLOT, G. & MATHIEU, J. 1971 Development of a turbulent boundary layer on a flat plate in an external turbulent flow. AGARD CP 93, No. 27.

CLIFT, R., GRACE, J. R. & WEBER, M. E. 1978 *Bubbles, Drops and Particles.* Academic Press, New York.

COLES, D. 1956 The law of the wake in turbulent boundary layer. *J. Fluid. Mech.* **1,** 191–226.

COLLIER, J. G. 1972 *Convective Boiling and Condensation,* pp. 382–406. McGraw-Hill, London.

DREW, D. A. & LAHEY, R. T. 1982 Phase-distribution mechanisms in turbulent low-quality two-phase flow in a circular pipe. *J. Fluid. Mech.* **117,** 91–106.

FERNHOLTZ, H. H. & VAGT, J. D. 1981 Turbulence measurements in an adverse pressure-gradient three-dimensional turbulent boundary layer along a circular cylinder. *J. Fluid. Mech.* **111,** 233–269.

HANCOCK, P. E. 1980 The effect of free-stream turbulence on turbulent boundary layers. Ph.D. Thesis, Imperial College, London (available on microfiche from the author).

HERRINGE, R. A. & DAVIS, M. R. 1976 Structural development of gas–liquid mixture flows. *J. Fluid. Mech.* **73,** 97–123.

ISHII, M. 1975 *Thermo-fluid Dynamic Theory of Two-phase Flow.* Eyrolles, Paris.

KADER, B. A. & YAGLOM, A. M., 1972 Heat and mass transfer laws for fully turbulent wall flows *Int. J. Heat Mass Transfer* **15,** 2329–2350.

KESTIN, J., MAEDER, P. F. & WANG, H. E. 1961 Influence of turbulence on the transfer of heat from plates with and without a pressure gradient. *Int. J. Heat Mass Transfer* **3,** 133–154.

LANCE, M. & BATAILLE, J. 1982 Turbulence in the liquid phase of a bubbly air–water flow. In *NATO Specialist's Meeting.* Martinus Nighoff, The Hague, The Netherlands.

LANCE, M., MARIÉ, J. L., CHARNAY, G. & BATAILLE, J. 1979 Les équations de la turbulence dans un écoulement diphasique incompressible en absence de transfert de masse. *C.r. Acad. Sci., Paris, Ser. A* **288,** 957–960.

LANCE, M., MARIÉ, J. L. & BATAILLE, J. 1984 Modélisation de la turbulence de la phase liquide dans un écoulement à bulles. *La Houille Blanche* **3,** 255–260.

LANCE, M., MARIÉ, J. L. & BATAILLE, J. 1985 Homogeneous turbulence in bubbly flows. Presented at *ASME Winter A. Mtg,* Miami Beach, Fla.

LEBOUCHÉ, M. & COGNET, G. 1967 La polarographie, moyen d'étude du mouvement des liquides. *Chimie Industrie-Génie Chimique* **97,** No. 12.

LOCKHART, R. W. & MARTINELLI, R. C. 1949 Proposed correlation of data for isothermal two-phase, two-component flow in pipes. *Chem. Engng Prog.* **45,** 39–48.

MARIÉ, J. L. 1983 Investigation of two-phase bubbly flows using laser Doppler anemometry. *PCH Jl* **4,** 103–108.

MARTINELLI, R. C. & NELSON, D. B. 1948 Prediction of pressure drop during forced circulation boiling of water. *Trans. ASME* **79,** 695–702.

MICHIYOSHI, I. 1978a Two-phase two-component heat transfer. *Proc. 6th Int. Heat Transfer Conf., Toronto* **7,** 219–233.

MICHIYOSHI, I. 1978b Heat transfer in air–water two-phase flow in a concentric annulus. *Proc. 6th Int. Heat Transfer Conf., Toronto* **1,** 499–504.

MICHIYOSHI, I. & SERIZAWA, A. 1984 Turbulence in two-phase bubbly flows. Presented at *Japan/U.S. Semin. on Two-Phase Flow Dynamics,* Lake Placid, N.Y.

OHBA, K., KISHIMOTO, I. & OGAZAWARA, M. 1976 Simultaneous measurement of local liquid velocity and void fraction in bubbly flows using a gas laser. *Tech. Rep. Osaka Univ.* **26,** 547–556.

ROBERTSON, J. M. & HOLT, C. F. 1972 Stream turbulence effects on turbulent boundary layers. *J. hydraul. Div. Proc. ASCE* **98**(HY6), 1095–1099.

SATO, Y., SADATOMI, M. & SEKOGUCHI, K. 1981 Momentum and heat transfer in two-phase bubble flow, Parts I & II. *Int. J. Multiphase Flow* **7**, 167–190.

SCHLICHTING, H. 1960 *Boundary Layer Theory*. McGraw-Hill, New York.

SERIZAWA, A., KATAOKA, I. & MICHIYOSHI, I. 1975 Turbulence structure of air-water bubbly flows. Part II: local properties. *Int. J. Multiphase Flow* **2**, 235–246.

SIMONICH, J. C. & BRADSHAW, P. 1978 Effect of a free-stream turbulence on heat transfer through a turbulent boundary layer. *ASME Jl Heat Transfer* **100**, 671–677.

SOUHAR, M. 1979 Etude du frottement pariétal dans les écoulements diphasiques en conduite verticale, cas des régimes à bulles et à poches. Thèse de Docteur-Ingénieur, Institut National Polytechnique de Lorraine, France.

SOUHAR, M. 1981 Contribution à l'étude dynamique des écoulements diphasiques gaz-liquide en conduite verticale: cas des régimes à bulles et à poches. Thèse d'Etat, Institut National Polytechnique de Lorraine, France.

TENNEKES, H. & LUMLEY, J. L. 1972 *A First Course in Turbulence*, pp. 146–196. MIT Press, Cambridge, Mass.

VAN DER WELLE, R. 1981 Turbulence viscosity in vertical adiabatic gas–liquid flow. *Int. J. Multiphase Flow* **7**, 461–473.

VAN DER WELLE, R. 1985 Void fraction, bubble velocity and bubble size in two-phase flow *Int. J. Multiphase Flow* **11**, 317–345.

WALLIS, G. B. 1969 *One-dimensional Two-phase Flow*. McGraw-Hill, New York.

ZUBER, N. & FINDLAY, J. A. 1965 Average volumetric concentration in two-phase flow systems. *J. Heat Transfer* **87**, 453–468.

ZUBER, N. & HENCH, J. 1962 Steady state and transient void fraction of bubbling systems and their operating limit: Part I. Steady state operation. General Electric Report 62 GL 100.

APPENDIX

Extension of the Usual Dimensional Analysis for the Core Region

Let consider the momentum equation in the longitudinal direction. For a steady fully-developed two-phase flow, it reduces (Drew & Lahey 1982) to

$$0 = -\frac{1}{\rho_L}\frac{d\overline{P_L}^x}{dZ} + \frac{1}{r}\frac{d}{dr}r\left[-(1-\alpha)\overline{u_L v_L}^x + \nu_L(1-\alpha)\frac{d\overline{U_L}^x}{dr}\right] - g(1-\alpha), \qquad [A.1]$$

where Z = axial coordinate, $r = R - Y$ = radial coordinate, $\overline{P_L}^x$ = phasic average of the pressure and $\overline{u_L v_L}^x$ = phasic average of the Reynolds stress. Elimination of $d\overline{P_L}^x/dZ$ and integration from 0 to r yields

$$-(1-\alpha)\overline{u_L v_L}^x + \nu_L(1-\alpha)\frac{d\overline{U_L}^x}{dr} = -\frac{r}{R}U_L^{*2} + g\langle\alpha\rangle\frac{r}{2} - \frac{g}{r}\int_0^r \alpha r\, dr, \qquad [A.2]$$

where $\langle\alpha\rangle$ is defined by $\langle\alpha\rangle = 1/\pi R^2 \int_0^R 2\pi r\,\alpha\, dr$.

In the core region, the viscous stress is negligible and [A.2] is approximated by

$$-(1-\alpha)\overline{u_L v_L}^x = -\frac{r}{R}U_L^{*2} + g\langle\alpha\rangle\frac{r}{2} - \frac{g}{r}\int_0^r \alpha\, r\, dr. \qquad [A.3]$$

We deduce that $(1-\alpha)\overline{u_L v_L}^x \to U_L^{*2}$ in the limit as $r \to R$. In other words, there is a subregion located approximately between $r/R = 0.7$ and 0.9, i.e. at the outer edge of the wall layer, where $\overline{u_L v_L}^x$ is likely of order U_L^{*2}. Unfortunately, we have no explicit information on $\overline{U_L}^x$ itself within this subregion. So we must examine another equation, e.g. that describing the turbulent energy budget in the boundary layer. According to the formulation by Lance *et al.* (1979) this equation is expressed by

$$-(1-\alpha)\overline{u_L v_L}^x\frac{d\overline{U_L}^x}{dr} + \overline{P_B} = (1-\alpha)\overline{\epsilon_L}^x + \frac{1}{r}\frac{d}{dr}r(1-\alpha)\left(\frac{\overline{p_L v_L}^x}{\rho_L} + \frac{\overline{q_L v_L}^x}{2}\right). \qquad [A.4]$$

The turbulent kinetic energy, called q_L, has mainly two origins. One part is generated by the Reynolds stress $-\overline{u_L v_L}^x$. The other part is produced by the bubbles. This production, whose rate

is denoted by $\overline{P_B}$, involves two mechanisms. The one is associated to the bubble wakes, the other to the acceleration of the liquid surrounding the interfaces. When the bubbles have reached their terminal velocity, which is the case here, both mechanisms are steady and it follows that $\overline{P_B}$ is constant. Moreover, as observed by Lance *et al.* (1985), $\overline{P_B}$ is exactly balanced by the rate $\overline{\epsilon_B}^x$ of viscous dissipation which occurs in the boundary layers around the bubbles and in their wakes. This suggests that the total disipation rate $\overline{\epsilon_L}^x$ is the sum of two statistically independent contributions, respectively $\overline{\epsilon_B}^x$ and the viscous dissipation rate $\bar{\epsilon}^x$ of the structures generated by the stress $-\overline{u_L v_L}^x$. From these arguments, we can write

$$-(1-\alpha)\,\overline{u_L v_L}^x \frac{d\overline{U_L}^x}{dr} = (1-\alpha)\bar{\epsilon}^x + \frac{1}{r}\frac{d}{dr} r(1-\alpha)\left(\frac{\overline{p_L v_L}^x}{\rho_L} + \frac{\overline{q_L v_L}^x}{2}\right). \qquad [A.5]$$

In this equation, as in [A.4], the viscous transport of $1/2\ q_L$ has been neglected. Consequently, we disregard the case where the turbulent Reynolds number is low. Having underlined this point, we estimate the order of magnitude of the remaining terms in the forementioned subregion. We know from [A.3] that the Reynolds stress $-\overline{u_L v_L}^x$, and hence the kinetic energy that it produces, is of order U_L^{*2}. Let us define L_B^s as the length scale of the eddies containing this energy and $\tilde{u}_B^s$ as the velocity scale of the fluctuations created by the bubbles. We may expect $\bar{\epsilon}^x$ to be of order U_L^{*3}/L_B^s and q_L of order $U_L^{*2} + \tilde{u}_B^{s2}$. Then the transport term (on the r.h.s. of [A.5]), which is of order $q_L^{1/2}/R$ times q_L, must be of order $(U_L^{*2} + \tilde{u}_B^{s2})^{3/2}/R$. Since the bubbles tend to break the large eddies, L_B^s is likely to be smaller than its corresponding value without gas, i.e. smaller than the pipe radius R. Thus in the sub-region, the action of the bubbles on the wall turbulence is described by two adimensional groups L_B^s/R and $\tilde{u}_B^s/U_L^*$. We conclude from [A.5] that the mean velocity gradient must also depend on these groups. By integration we deduce that the defect velocity profile in the subregion must be of the form

$$\frac{\overline{U_L^0}^x - \overline{U_L}^x}{U_L^*} = F\left(\eta, \frac{L_B^s}{R}, \frac{\tilde{u}_B^s}{U_L^*}\right). \qquad [A.6]$$